

ARTICLE OPEN



Genome wide CRISPR/Cas9 screen identifies the coagulation factor IX (F9) as a regulator of senescence

Paula Carpintero-Fernández^{1,6}, Michela Borghesan¹, Olga Eleftheriadou¹, Belen Pan-Castillo^{1,2}, Juan Antonio Fafián-Labora^{1,7}, Tom P. Mitchell³, Alejandro Yuste⁴, Muge Ogrunc^{2,5}, Thomas D. Nightingale³, Maria Mayan⁴ and Ana O’Loghlen¹✉

© The Author(s) 2022

During this last decade, the development of pro-senescence therapies has become an attractive strategy as cellular senescence acts as a barrier against tumour progression. In this context, CDK4/6 inhibitors induce senescence and reduce tumour growth in breast cancer patients. However, even though cancer cells are arrested after CDK4/6 inhibitor treatment, genes regulating senescence in this context are still unknown limiting their antitumour activity. Here, using a functional genome-wide CRISPR/Cas9 genetic screen we found several genes that participate in the proliferation arrest induced by CDK4/6 inhibitors. We find that downregulation of the coagulation factor IX (*F9*) using sgRNA and shRNA prevents the cell cycle arrest and senescent-like phenotype induced in MCF7 breast tumour cells upon Palbociclib treatment. These results were confirmed using another breast cancer cell line, T47D, and with an alternative CDK4/6 inhibitor, Abemaciclib, and further tested in a panel of 22 cancer cells. While *F9* knockout prevents the induction of senescence, treatment with a recombinant *F9* protein was sufficient to induce a cell cycle arrest and senescence-like state in MCF7 tumour cells. Besides, endogenous *F9* is upregulated in different human primary cells cultures undergoing senescence. Importantly, bioinformatics analysis of cancer datasets suggest a role for *F9* in human tumours. Altogether, these data collectively propose key genes involved in CDK4/6 inhibitor response that will be useful to design new therapeutic strategies in personalised medicine in order to increase their efficiency, stratify patients and avoid drug resistance.

Cell Death and Disease (2022)13:163; <https://doi.org/10.1038/s41419-022-04569-3>

INTRODUCTION

A key characteristic of cancer cells is the deregulation of cyclin-dependent kinases (CDKs) leading to uncontrolled cell proliferation. Consequently, CDK4/6 inhibitors (Abemaciclib, Palbociclib and Ribociclib) induce senescence in vitro and in vivo [1–7]. Cellular senescence is defined as a state in which cells lose their proliferative capacity. They differ from dividing cells in terms of gene expression, chromatin structure and metabolism. Senescent cells also comprise a complex inflammatory response known as senescence-associated secretory phenotype (SASP) [8–10]. The SASP is characterised by the secretion of cytokines, enzymes, chemokines and extracellular vesicles that cause inflammation and is pivotal for the clearance of senescent cells by the immune system [11, 12]. However, the role the senescent plays during cancer is still under debate, with some studies showing its beneficial effects as a tumour suppressor mechanism, but others demonstrating it promotes tumorigenesis [8, 9, 13, 14].

CDK4/6 inhibitors induce senescence by inhibiting the phosphorylation of retinoblastoma (RB1), stabilising the RB-E2F inhibitory complex and preventing the activity of E2F transcription factors that regulate cell cycle progression [15–17]. Although initially thought to provide promising clinical outcomes due to their specificity and sensitivity for CDK4/6, resistance or intrinsic lack of response to these inhibitors has limited their clinical success [18, 19]. Thus, the molecular mechanisms by which CDK4/6 inhibitors induce senescence in cancer cells and the genes involved in conferring drug resistance or lack of response to these inhibitors are unknown, preventing patient stratification prior to Palbociclib treatment [18].

In this study, using a human genome-wide CRISPR/Cas9 library we identified genes whose loss-of-function prevent the proliferative arrest induced by Palbociclib in MCF7 breast cancer cells. Validation of the CRISPR/Cas9 screen using additional sgRNA and shRNA confirmed that among the identified genes, the coagulation factor IX (*F9*) participates in the cell cycle arrest induced by

¹Epigenetics & Cellular Senescence Group; Blizard Institute; Barts and The London School of Medicine and Dentistry; Queen Mary University of London; 4 Newark Street, London E1 2AT, United Kingdom. ²StarkAge Therapeutics, Campus de l’Institut Pasteur de Lille, 1 rue du Professeur Calmette, 59800 Lille, France. ³Centre for Microvascular Research. The William Harvey Research Institute. Charterhouse Square Barts and the London School of Medicine and Dentistry Queen Mary University of London, EC1M 6BQ, London, UK. ⁴CellCOM Research Group. Instituto de Investigación Biomédica de A Coruña (INIBIC). CH-Universitario A Coruña (XXIAC). Universidade da Coruña. Servizo Galego de Saúde (SERGAS). Xubias de Arriba, 84 15006 A Coruña, Spain. ⁵SynLab Hauts-de-France, Campus de l’Institut Pasteur de Lille, 1 rue du Professeur Calmette, 59800 Lille, France. ⁶Present address: CellCOM Research Group. Instituto de Investigación Biomédica de A Coruña (INIBIC). CH-Universitario A Coruña (XXIAC), Universidade da Coruña. Servizo Galego de Saúde (SERGAS) Xubias de Arriba, 84 15006A Coruña, Spain. ⁷Present address: Grupo de investigación en Terapia Celular y Medicina Regenerativa, Departamento de Fisioterapia, Medicina y Ciencias Biomédicas, Facultad de Ciencias de la Salud, Universidade da Coruña, INIBIC-Complejo Hospitalario Universitario A Coruña (CHUAC), Agrupación estratégica CICA-INIBIC, As Xubias, 15006 A Coruña, Spain. ✉email: a.ologhlen@qmul.ac.uk

Edited by Dr Ivano Amelio

Received: 8 April 2021 Revised: 22 December 2021 Accepted: 17 January 2022

Published online: 19 February 2022

Palbociclib. These results were confirmed using Abemaciclib, where we saw that downregulation of *F9* also prevented the induction of senescence. Meanwhile, treatment with recombinant *F9* induced a senescence-like proliferative arrest in MCF7 cells but not in cancer cells which did not upregulate *F9* upon Palbo treatment. Our results demonstrate that *F9* is endogenously upregulated upon activation of senescence by different triggers in human primary fibroblasts and endothelial cells. Finally, we screened a panel of 22 cancer cell lines for their response to different CDK4/6 inhibitors and we show that *F9* loss-of-function confers a partial resistance to the proliferative arrest induced by CDK4/6 inhibitors in other tumour types. Analyses of published datasets suggest a role for *F9* in carcinogenesis in different tumours in humans. Importantly, our results open new therapeutic opportunities with the potential to stratify patients for CDK4/6 inhibitors response prior to treatment.

RESULTS

A CRISPR/Cas9 genome-wide screen identifies genes overcoming the proliferative arrest induced by Palbo

To identify genes whose loss-of-function overcome the proliferative arrest induced by Palbociclib (PD-0332991 or Palbo) we performed a CRISPR/Cas9 screen using the human genome-wide library GeCKOv2 [20, 21]. This library contains ~123,441 unique sgRNA targeting 19,050 genes in the human genome with a coverage of 5–6 sgRNA per gene (Fig. 1A). To confirm that Palbo induces senescence we treated MCF7 ER⁺ breast cancer cells with increasing concentrations (0.1, 0.2, 0.5 and 1 μM) for 7 and 14 days and analysed several biomarkers of senescence [11]. We confirmed that Palbo induced a stable cell cycle arrest by quantifying the number of cells staining positive for BrdU and by quantifying cell number (Fig. S1A). Palbo treatment induced an increase in β-Galactosidase activity (SA-β-Gal), a common characteristic of senescence (Fig. S1B). Neither of the doses used induced apoptosis quantified by measuring the number of cells staining positive for AnnexinV (Fig. S1C). We determined additional markers of senescence by treating MCF7 with 200 nM Palbo during 14 days and confirmed an increase in SA-β-Gal activity and in the number of cells staining positive for p21^{CIP} by immunofluorescence (IF) (Fig. S1D–F). Next, we infected MCF7 cells with a single-vector lentiviral construct (comprising sgRNA and Cas9 in a single vector), lentiCRISPRv2, (Fig. S1G) or containing the GeCKO pooled library and treated them with DMSO or 200 nM Palbo for 14 days (Fig. 1A). MCF7 cells were plated at low density where an advantage in proliferation could be observed upon the expression of the GeCKO library (Fig. 1B). Enrichment of sgRNAs after two weeks Palbo treatment compared to day 0 was determined by genomic DNA extraction and deep sequencing as previously described [20, 21] (Fig. 1C). Among all the sgRNA enriched after two weeks treatment ($p < 0.05$) we selected: (i) single sgRNA enriched $\geq 2 \log_2$ fold change RPKM between day 0 and 14 and, (ii) those sgRNA where we found ≥ 3 individual sgRNA per gene preventing the proliferative arrest. A list of 18 potential genes whose loss-of-function prevent the cell cycle arrest induced by Palbo (Fig. 1D) were subjected to KEGG (Kyoto Encyclopedia of Genes and Genomes) pathway and STRING protein interaction analysis and two genes associated with the blood coagulation pathway were highlighted: the coagulation factor IX (*F9*) and Protein Z Vitamin K Dependent Plasma Glycoprotein (*PROZ*) (Fig. 1D–F). Enrichment of individual sgRNA within the GeCKO library belonging to the coagulation pathway (5 sgRNAs for *PROZ* and 6 sgRNA for *F9*) with $\geq 2 \log_2$ fold change RPKM after two weeks Palbo treatment show a statistical difference (Fig. 1G). Altogether, these data propose 18 candidate genes whose loss-of-function prevent the proliferation arrest induced by Palbo with an overrepresentation of two genes involved in the blood coagulation pathway.

F9 and *PROZ* loss-of-function prevent the proliferation arrest induced by Palbo

To validate the implication of *F9* and *PROZ* we designed and cloned 4 additional sgRNA targeting *PROZ* (sgPROZ) or *F9* (sgF9) (Fig. 2A). We included an sgRNA targeting *RB1* (sgRB) as a control [22]. MCF7 cells were infected with 4 pooled sgRNAs targeting each candidate gene and treated with DMSO or 200 nM Palbo. The ability of sgF9, sgPROZ and sgRB to prevent the proliferation arrest induced by Palbo was confirmed by performing proliferation curves at different days after treatment (Fig. 2B, C). The efficacy of the sgRNAs were assessed at the mRNA (Fig. S2A) and protein level for RB (Fig. S2B). Importantly, MCF7 basal proliferation was not affected by sgF9 or sgPROZ expression alone, confirming that the bypass in proliferation was specific to sgF9 and sgPROZ upon Palbo treatment (Fig. 2D). Next, we hypothesised that *F9* and *PROZ* were upregulated during senescence, and thus, their loss-of-function was the cause of the lack of response to Palbo. Indeed, we could observe an increase in the mRNA expression levels of *F9* and *PROZ* in MCF7 cells after 20 days Palbo treatment (Fig. 2E). To determine whether *F9* could be secreted as part of the SASP, we performed an ELISA assay and confirmed an increase in the amount of *F9* released upon Palbo treatment (Fig. 2F). Furthermore, an increase in the protein levels of *F9* could also be detected by IF (Fig. 2G).

We next wanted to corroborate that the proliferation arrest upon Palbo treatment was stable and that both sgPROZ and sgF9 were implicated in bypassing this arrest. MCF7 cells were treated with Palbo for 6 days, washed and cultured in the absence of the drug until day 20 (Fig. S2C). As shown in Fig. S2D treatment of MCF7 cells with Palbo resulted in a stable inhibition of proliferation even in the absence of the drug as shown by low-density plating and CV staining (Fig. S2D).

F9 loss-of-function prevents the senescence-like phenotype induced by Palbo

We decided to focus on *F9* knockout as its proliferation bypass is stronger than sgPROZ (Fig. 2C). We thus determined whether this proliferative advantage was maintained using different concentrations of Palbo. We treated MCF7 cells with 200 nM and 500 nM Palbo for 20 days and counted cell numbers at day 20 (Fig. S2E). The knockout efficiency of sgF9 and sgRB was validated at day 20 to ensure that plasmid expression was not lost (Fig. S2F). sgF9 bypass was also shown by quantifying the percentage of cells staining positive for Ki67 by IF (Fig. 2H, I) and low-density cell plating (Fig. S2G), with no changes in the apoptosis marker AnnexinV (Fig. S2H).

We next tested whether sgF9 could be inducing an increase in the migration capacity of MCF7 cells, thus promoting tumorigenesis. However, we show a decrease in the relative number of MCF7 cells migrating upon 500 nM Palbo treatment for 20 days which is not prevented by sgF9 (Fig. S2I). MDA-MB-468 cells were used as a control.

To exclude the potential implication of off-target effects derived from using CRISPR/Cas9, we infected MCF7 cells with two independent viral constructs carrying an shRNA targeting *F9* (shF9#3 and shF9#4). Both shF9 constructs recapitulated the effects observed with sgF9 measured by quantifying the number of cells staining positive for BrdU (Fig. 2J, K). *F9* downregulation was confirmed at the mRNA level by qPCR (Fig. S2J). Altogether, these data show that *F9* loss-of-function using genome editing and RNAi interference overcomes the cell cycle arrest induced by Palbo in MCF7 cells.

F9 is endogenously upregulated during senescence

We set to determine the importance of *F9* expression during senescence; thus, we evaluated whether sgF9 prevented the induction of other features of senescence such as the SASP. sgF9 downregulates several SASP mRNA transcripts upregulated by

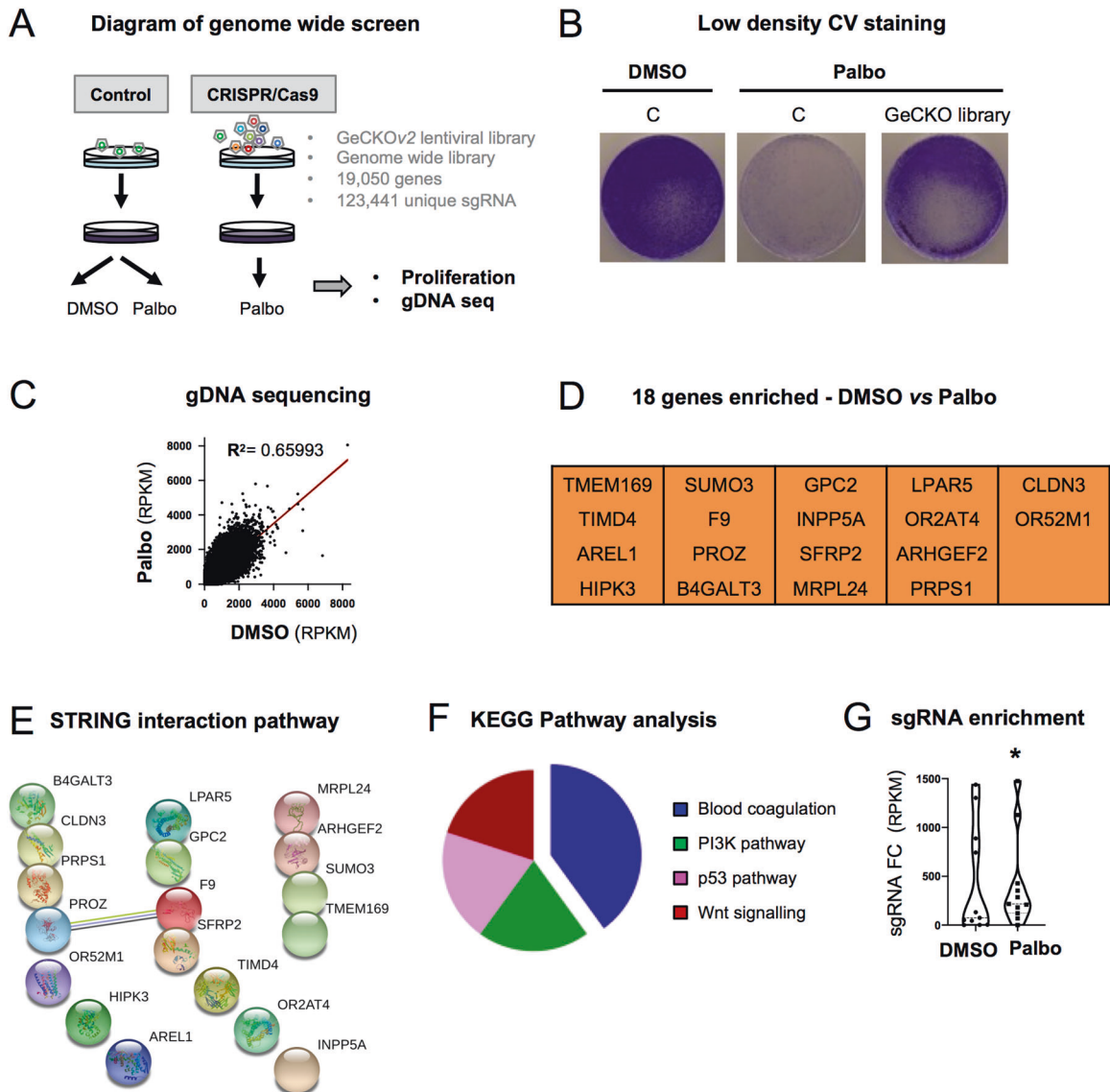
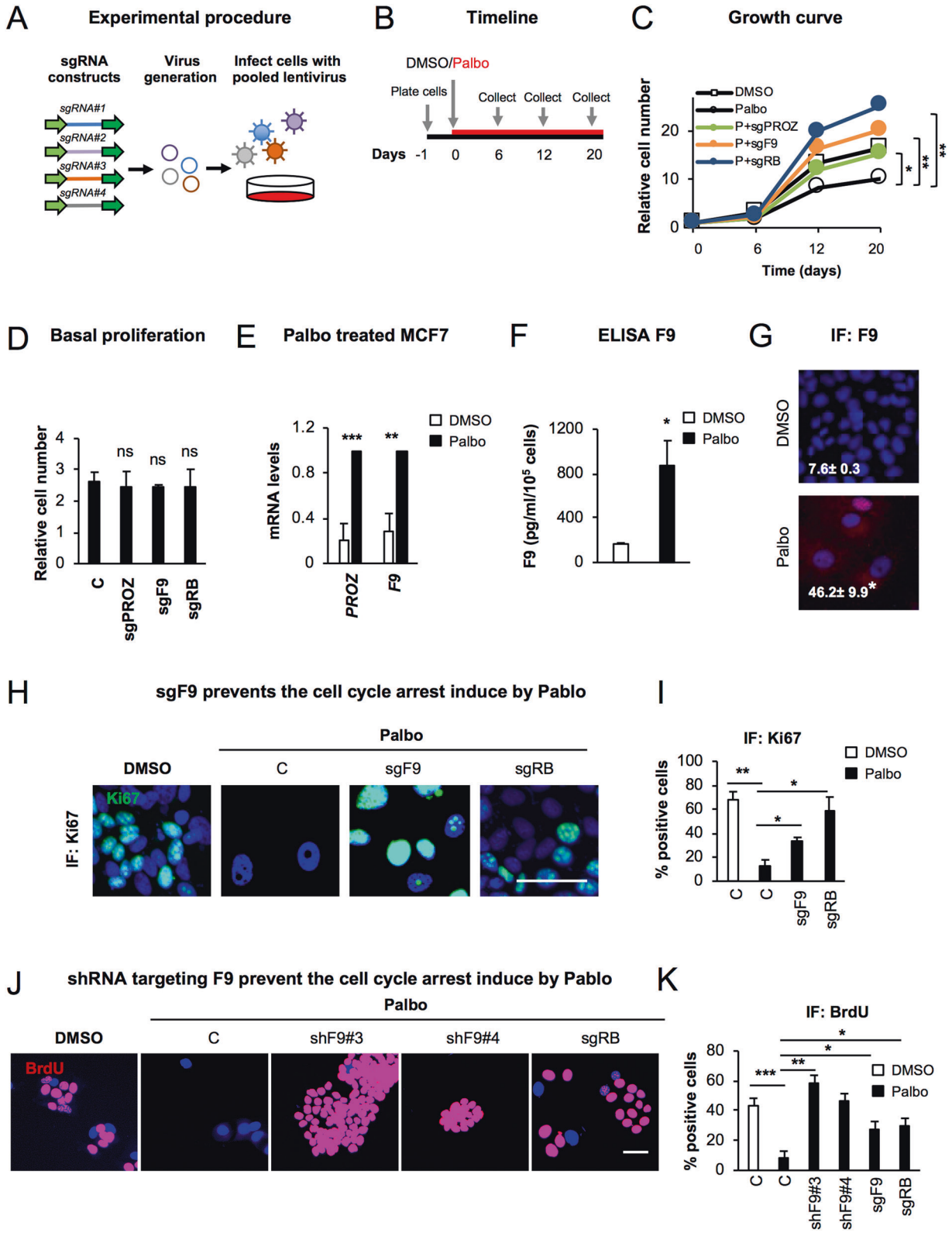


Fig. 1 CRISPR/Cas9 screening identifies candidate genes whose loss are implicated in Palbociclib cell cycle arrest. **A** Schematic representation of the proof-of-concept genome-wide screen performed in MCF7 cells using the GeCKOv2 pooled sgRNA library. Cells were infected with the library (CRISPR/Cas9) or the control (control), selected with puromycin and treated with 200 nM of Palbociclib (Palbo) for 14 days. **B** MCF7 cells expressing either the control (C) or the GeCKO library after 14 days of 200 nM Palbo treatment were stained with crystal violet. A representative experiment of 2 independent experiments is shown. **C** Genomic DNA (gDNA) sequencing data showing the enrichment of sgRNA after two weeks of 200 nM Palbo treatment. Data show a representative experiment from 2 independent experiments. Statistically significant ($p < 0.05$) transformed RPKM is shown. **D** sgRNA targeting 18 different genes were found to be statistically significant following the selection criteria of: (i) >2 FC (fold change) differential expression between DMSO and day 14 Palbo treatment and, (ii) 3 or more sgRNA conferring a proliferative advantage. **E** STRING protein interaction and **F** Kyoto Encyclopedia of Genes and Genomes (KEGG) analysis for the 18 genes whose sgRNA were enriched after 14 days Palbo treatment in panel D. **G** Violin plot showing all individual sgRNA within the GECKO library related to the coagulation pathway (5 sgRNAs for *PROZ* and 6 sgRNA for *F9*) enriched after two weeks Palbo treatment (FC, fold change RPKM). Median for values is shown for all sgRNA from 2 independent experiments. One sample t and Wilcoxon test was performed. Related to Fig. S1.

Palbo such as *MMP9*, *MMP3*, *IL1B* and *IL6* while having no effect on *CCL20*, *IL1A* or *IL8* (Fig. 3A). Importantly, sgRB averted the endogenous upregulation of *F9* mRNA levels (Fig. 3B), suggesting that *F9* mRNA expression is dependent on RB.

Next, we took advantage of human primary fibroblasts (HFFF2) expressing an endoplasmic reticulum (ER):H-RAS^{G12V} fusion protein (iRAS) where 200 nM 4-hydroxytamoxifen (4OHT) treatment for 6 days induces senescence [6, 12]. In fact, we observe a consistent upregulation of endogenous *F9* mRNA during OIS (Fig. 3C) concomitant with an increased SA- β -gal activity (Fig. S3A). This was recapitulated in HFFF2 treated with 50 μ M etoposide for 2 days and

collecting RNA at day 7, mimicking DNA-damage-induced senescence (DDIS). Moreover, treatment of HFFF2 fibroblasts with 1 μ M Palbo for 7 days, mirroring therapy-induced senescence (TIS), also triggered the endogenous upregulation of *F9* mRNA (Fig. 3C). Confirmation of the induction of senescence was further demonstrated by showing a reduction in cell proliferation measured by quantifying cell number and an increase in the number of SA- β -gal positive cells (Fig. S3B, C) [6, 12, 23]. Activation of senescence and endogenous upregulation of *F9* was also observed in human umbilical vein endothelial cells (HUVEC). HUVEC cells treated with 500 nM Palbo for 7 days showed an increase in the percentage of



cells staining positive for F9 by IF (Fig. 3D, E) concomitant with reduced proliferation, an increase in p21^{CIP1} and an increase in the levels of secreted F9 (Fig. S3D-F).

Finally, ectopic administration of 10µg/mL recombinant F9 protein (rF9) twice during 6 days induced a senescence-like phenotype in MCF7 cells shown by a reduction in cell numbers, a

decrease in BrdU incorporation, an increase in p21^{CIP1} positive cells associated with increased SA-β-Gal activity (Fig. 3F-H). Interestingly, treatment of the melanoma cell line SKMEL28, which does not upregulate F9 upon Palbo treatment, (Fig. S3G) failed to induce a significant increase in p21^{CIP1} upon rF9 treatment in spite of showing a proliferation arrest as presented in Fig. S3H.

Fig. 2 CRISPR/Cas9 screen validation identifies *F9* as a regulator of the proliferation arrest induced by Palbo. **A** Schematic representation of the viral production for the CRISPR/Cas9 screen validation. 4 sgRNA targeting the same gene (e.g. *PROZ* or *F9*) were pooled and used to infect MCF7 cells. **B** Overview of the experimental set-up followed to validate the identified sgRNA. Briefly, after plating, MCF7 infected cells were treated with 200 nM Palbo and samples were collected to determine cell number at days 6, 12 and 20 after Palbo treatment. **C** MCF7 cells expressing the indicated sgRNAs were treated with 200 nM Palbo for 20 days and collected at different time points (0, 6, 12, 20 days) to assess proliferation. Proliferation curves show that MCF7 expressing sgF9 (orange line) and sgPROZ (green line) prevented a stable cell cycle arrest compared to Palbo (P) treated cells (black line - circles). sgRB MCF7 cells treated with Palbo (blue line) were used as a positive control. The data represent the mean of 4 independent experiments for C, Palbo and sgPROZ and 3 for sgF9 and sgRB. Student's t-test analysis at day 20 was performed compared to the Palbo treated sample. **D** Basal proliferation rate was determined by quantifying nuclei count after sgRNA infection at 20 days of cell culture. Data show the mean \pm SEM of 3 independent experiments for C, sgF9 and 2 for sgPROZ and sgRB. Two-tailed student's t-test compared to the C sample was performed. **E** MCF7 treated with Palbo for 20 days induce an upregulation of *F9* and *PROZ* mRNA levels as shown by qPCR analysis. Data represent the mean \pm SEM of 5 independent experiments. Two-tailed t-test analysis was performed. **F** ELISA for F9 protein levels secreted by MCF7 cells upon DMSO or Palbo treatment for 20 days. Data represent the mean \pm SEM of 4 independent experiments. Two-tailed t-test was performed. **G** Representative images and quantification for F9 staining in MCF7 cells treated with 500 nM Palbo for 7 days. Data represent the mean \pm SEM of 3 independent experiments. Two-tailed t-test was performed. **H, I** (**H**) Representative images and **I** quantification showing that sgF9 prevents the proliferation arrest induced by Palbo by displaying an increase in the percentage of cells staining positive for Ki67 (green). Data show the mean \pm SEM of 3 independent experiments. Two-tailed t-test analysis comparing to Palbo sample was performed. Scale bar: 50 μ m. **J, K** (**J**) Representative images and **K** quantification for BrdU staining of MCF7 cells infected with a construct expressing two individual shRNA targeting *F9* (shF9#3 and shF9#4). sgF9 and sgRB are used as a positive control. Scale bar: 50 μ m. Data show the mean \pm SEM of 3 independent experiments. Two-tailed students t-test compared to the Palbo sample was performed. See also Fig. S2.

Altogether, these data highlight the implication of *F9* in inducing senescence using a variety of triggers in different human primary cell cultures and the implication of the induction of senescence upon treatment with rF9.

***F9* regulates senescence in MCF7 cells treated with Abema and in T47D**

Next, we wanted to determine whether the proliferation bypass by sgF9 was due to the specific inhibition of CDK4/6 and not due to off-target effects. For this, we used increasing concentrations (0.25, 1 and 5 μ M) of Abemaciclib (Abema) or Ribociclib (Ribo), including Palbo as a positive control (Fig. 4A, B). We could observe a dose-dependent cell cycle arrest upon treatment with other CDK4/6 inhibitors (Abema in particular) concomitant with a decrease in RB protein levels (Fig. 4B, Fig. S4A) which was maintained after 14 days of continuous treatment (Fig. S4B, C). We next confirmed the induction of a stable cell cycle arrest characteristic of senescence by treating MCF7 cells for 6 days with Abema, Palbo or Ribo, withdrawing the inhibitors and leaving for 14 further days after the drug removal (Fig. S4D). Our data confirm that both Palbo and Abema induce a stable cell cycle arrest even after drug withdrawal which was not maintained when the cells were treated with Ribo (Fig. S4D). In line with our previous results, *F9* mRNA levels increased when MCF7 cells were treated with Palbo and Abema but not with Ribo (Fig. 4C). We treated sgF9 MCF7 cells with 1 μ M Abema for 20 days and show that it partially prevented the cell cycle arrest by Ki67 (Fig. 4D) and by crystal violet staining (Fig. S4E). Furthermore, we determined the implication of sgF9 using another ER⁺ (T47D) and the triple-negative (MDA-MB-468) breast cancer cell lines. sgF9 prevented the cell cycle arrest induced by Palbo in T47D cells as shown by colony formation assay (Fig. 4E) and by counting cell numbers (Fig. 4F). The knockout efficiency for *RB* and *F9* was determined at the protein level for RB (Fig. S4F) and RNA levels for *RB* and *F9* (Fig. S4G). However, MDA-MB-468 cells did not respond to Palbo treatment as previously reported [15] (Fig. 4E) in spite of *F9* and *RB* being downregulated (Fig. S4H) by their respective sgRNAs. The induction of senescence by Palbo in T47D was further confirmed by measuring SA- β -Gal activity (Fig. 4G) and the release of F9 by ELISA (Fig. 4H). The implication of sgF9 was further validated using two independent shF9#3 and shF9#4 by colony formation assay (Fig. S4I), relative cell count (Fig. S4J) and F9 secretion (Fig. 4H). Confirmation of the knockdown efficiency was confirmed by qPCR (Fig. S4K). Altogether, these data show that *F9* loss prevents the induction of senescence by treatment with Palbo and Abema in T47D cells.

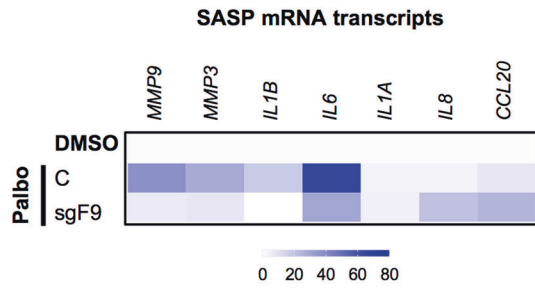
Other cancer cell lines respond to CDK4/6 inhibitors and induce *F9* upregulation

To further determine if there is a wider implication for *F9* loss-of-function in other types of cancers, we tested a panel of 22 cancer cell lines from different origins and molecular characteristics with increasing concentrations of Palbo, Abema and Ribo (Fig. 5A, Fig. S5A). 8 cancer cell lines (including MCF7) responded to ≥ 2 CDK4/6 inhibitors in a dose-dependent and statistically significant manner ($p < 0.05$) (Fig. 5B). Further validation of these 8 cell lines in a secondary screen re-evaluating the proliferation arrest induced by all three CDK4/6 inhibitors confirmed the response of 5 cell lines ($p < 0.05$) to ≥ 2 CDK4/6 inhibitors (MCF7, SKMEL28, ACHN, HT-29, SNU-387) (Fig. 5C, Fig. S5B, C). Next, we determined which of these 5 cell lines (excluding MCF7) induced an upregulation of endogenous *F9* mRNA levels upon the treatment with all three inhibitors by qPCR. Of all the cancer cell lines analysed, the renal adenocarcinoma cell line (ACHN) was the only cell line to upregulate *F9* with Palbo and Abema (Fig. 5D), while the human colorectal adenocarcinoma cell line (HT29) and the hepatocellular carcinoma cell (SNU-387) increased *F9* mRNA expression only with Palbo (Fig. 5D). *F9* was not upregulated by Ribo in any of the cell lines analysed (Fig. 5D). A partial proliferation bypass by crystal violet staining in ACHN upon shF9#4 expression was observed (Fig. 5E). This bypass could implicate that *F9* is only partially important in Palbo induced senescence in ACHN cells and that other mechanisms might be implicated. Altogether, our data highlight a partial relevance for *F9* mRNA expression in other cancer cell lines.

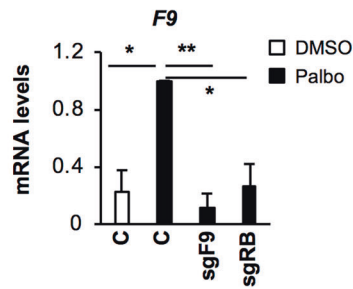
***F9* is highly expressed in the tumour stroma**

Next, we sought to explore public datasets of gene expression in the tumour stroma of several human cancers: GSE34312 (prostate) [24], GSE9014 (breast) [25], and GSE35602 (colon) [26]. We found that *F9* is upregulated in the tumour stroma in comparison with healthy stroma in breast and colon, but not in prostate cancer (Fig. 6A). When analysing other transcripts implicated in the intrinsic coagulation pathway where *F9* is involved, most are also upregulated in breast cancer, while transcripts within the extrinsic pathway are mainly downregulated (Fig. 6B) [27]. As the tumour microenvironment is composed of cancer cells and stroma, we next sought to identify whether a cross-talk existed between iRAS fibroblasts and MCF7 treated with DMSO or Palbo (Fig. 6C). Senescence was induced in iRAS cells with 200 nM 4OHT for 3 days, washed and incubated with fresh media after which the conditioned media (CM) was collected (Fig. 6C). MCF7 pre-treated with or without 500 nM Palbo for 7 days plus 3 days in 0.5% serum

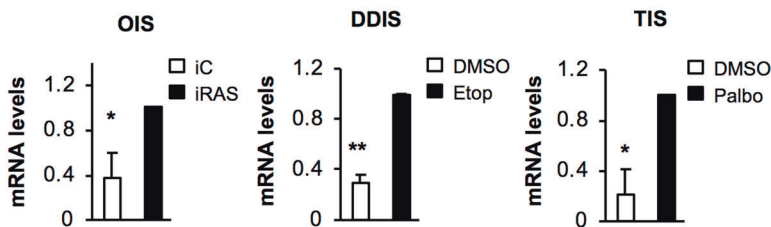
A sgF9 prevents Palbo-induced senescence



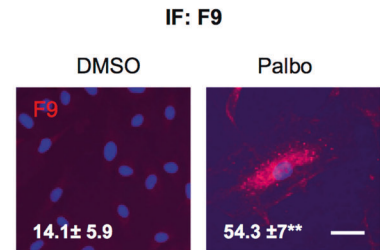
B F9 is not upregulated with sgRB



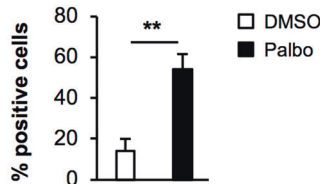
C F9 mRNA expression levels in senescent HFFF2



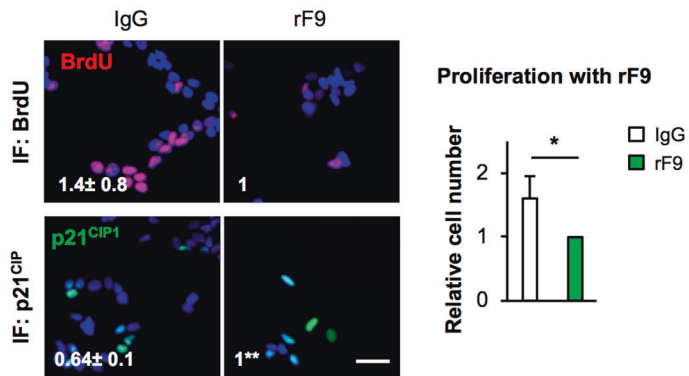
D F9 increase in senescent HUVEC



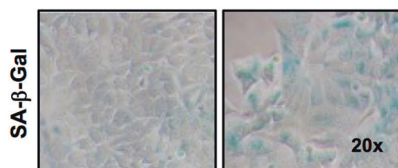
E IF: F9 protein levels HUVEC



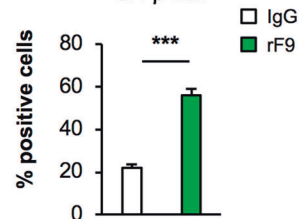
F F9 ectopic expression induces senescence in MCF7



G SA-β-Gal staining in MCF7 treated with rF9



H SA-β-Gal



were incubated with the CM from iRAS for 72h and we determined changes in F9 mRNA levels (Fig. 6D). Interestingly, we found a sharp increase in F9 mRNA levels when senescent MCF7 cells (pretreated with Palbo) were incubated with the CM of senescent iRAS (+4OHT). This increase also correlated with other

SASP mRNA transcripts (Fig. 6E) confirming previous studies highlighting that the SASP reinforces the cell cycle arrest and the induction of senescence [28]. The SASP of MCF7 cells (which express F9 upon the induction of senescence) also reinforced the senescence of Palbo-treated MCF7 and T47D (Fig. S6A, B).

Fig. 3 F9 induces senescence and it is endogenously upregulated during senescence. A Heat map of SASP mRNA levels in MCF7 cells control or expressing sgF9 after 20 days treatment with Palbo. The mean of 2–7 independent biological replicates is shown. **B** *F9* mRNA upregulation by Palbo is prevented when RB is not present (sgRB). Data show the mean \pm SEM of 4 independent experiments. One-WAY ANOVA with Dunnett's multiple comparison to Palbo sample was performed. **C** mRNA levels of endogenous *F9* mRNA levels in HFFF2 (human primary fibroblasts) upon the induction of senescence. OIS (Oncogene-induced senescence) was induced in HFFF2 expressing ER:H-RAS^{G12V} (iRAS) by adding 200 nM 4OHT for 6 days (left panel); 50 μ M etoposide was added for 2 days and washed out until day 7 to induce DDIS (DNA-damage senescence) (middle panel); TIS (Therapy-induced senescence) was mimicked by treating with 1 μ M of Palbo for 7 days (right panel). Data represent the mean \pm SEM of 3 independent experiments for OIS and DDIS and 2 for TIS. Two-tailed student's t-test analysis was performed. **D** Representative immunofluorescence images and **E** IF quantification showing the expression of endogenous *F9* (red) in HUVEC (human umbilical vein endothelial cells) upon 7 days treatment with 500 nM Palbo. Scale bar: 50 μ m. The data represent the mean \pm SEM of 4 independent experiments. Two-tailed student's t-test was used to calculate statistical significance. **F Left panel**, Representative images for BrdU (red) and p21^{CIP1} (green) in MCF7 treated twice with 10 μ g/mL of recombinant *F9* (rF9) for 6 days. Scale bar: 50 μ m. 3 independent experiments were performed. **Right panel**, The graph shows a reduction in the number of cells at the end of the experiment. Mean \pm SD of 3 independent experiments is shown. Two-tailed student's t-test was used to determine statistical significance. **G** Representative pictures and **H** quantification of MCF7 cells staining positive for SA- β -Gal activity when treated twice with 10 μ g/mL rF9. Data represent mean \pm SEM of 3 independent experiments. Two-tailed student's t-test was used. See also Fig. S3.

In contrast, when two cancer cell lines that did not upregulate *F9*, SKMEL28 (Fig. 5D) and MDA-MB-468 (Fig. S6C) were treated with the conditioned media of Palbo-treated MCF7 or iRAS cells, no differences could be observed in the levels of *F9* mRNA (Fig. S6D) in spite of *F9* mRNA levels being upregulated upon 4OHT treatment in iRAS cells (Fig. S6E). The same results could be observed upon treatment of SKMEL28 with the CM from MCF7 undergoing Palbo treatment or not (Fig. S6F). Altogether, these results highlighting the relevance of *F9* as a regulator of senescence induced by Palbo.

F9 loss-of-function is associated with metastasis and worse survival prognostics in cancer

Our data suggest that increased levels of *F9* upon the induction of senescence maintain certain cancer cells in a stable cell cycle arrest, while *F9* loss-of-function promotes a proliferative advantage. In accordance with our data, low levels of *F9* are associated with liver metastasis [29] (Fig. 6F). Importantly, high levels of *F9* expression are a sign of good prognostic for survival in breast cancer [30] (Fig. 6G). Interestingly, low expression levels of *F9* in different subtypes of breast cancer (basal, luminal A and luminal B) are also associated with poor prognosis and lower disease-free survival probability (Fig. S6G, I). Altogether, these data show the potential of using *F9* levels as a biomarker for patient stratification not only to predict response to CDK4/6 inhibitors but also as a prognostic marker to determine overall survival in breast cancer.

DISCUSSION

A better understanding of the mechanisms regulating senescence induced by CDK4/6 inhibitors is needed in order to increase therapy efficacy and patient stratification in cancer. In this study, by performing a whole genome-wide CRISPR/Cas9 screen, we have unveiled a role for the coagulation factor IX (*F9*) as an important regulator of senescence induced by CDK4/6 inhibitors in ER⁺ breast cancer cell lines and other cancer cells, thus identifying genes whose loss can predicted a lack of response to Palbo.

Previous publications have shown that inflammation, hypercoagulability and cellular senescence share common pathways [31]. In fact, a correlation between thrombosis and cancer [32–34] is well known, although the link with cellular senescence is less characterised. Interestingly, Wiley et al. demonstrated that human fibroblasts undergoing senescence secrete a subset of haemostasis-related factors as part of the SASP [35]. It is however curious to note that they did not find factors implicated in the coagulation pathway suggesting that maybe different triggers or cell types could favour either general haemostasis or the coagulation pathway specifically. Importantly, the combination of MEK and CDK4/6 inhibitors in pancreatic adenocarcinoma induce senescence including the release of SASP factors enriched

in pro-angiogenic proteins promoting tumour vascularisation and enhancing drug delivery and efficacy [7]. In line with these findings, senescent human primary fibroblasts also release pro-angiogenic factors such as VEGF [36]. Altogether, these findings, in conjunction with ours, show that *angiogenesis* and the coagulation pathway play an important role in senescence. In fact, the coagulation pathway has been shown to be upregulated in senescence [37] and ageing [38, 39]. Furthermore, *F9* has been associated with frailty [40] and is a genetic risk factor estimated to contribute to thrombosis incidence in the elderly [38, 41].

The expression of the oncogene *MET* in the liver in vivo causes hepatocarcinogenesis, blood hypercoagulation and internal bleeding [32]. In fact, the use of antiplatelet therapy in liver cancer prevents cross-talk between platelets and immune cells [42]. Curiously, chemotherapy treatment increases the risk of thrombosis [43] but it also induces senescence promoting cancer relapse [13]. Importantly, *F9* expression can induce regulatory CD4⁺ T cells in mice suggesting a role for *F9* in immunosurveillance [44]. It would therefore be interesting to further explore the implications of the coagulation pathway and *F9* in the context of chemotherapy and senescence immunosurveillance.

In summary, here we provide evidence for the involvement of two different genes within the coagulation pathway, *F9* and *PROZ*, in regulating senescence in different contexts. Our results show that *F9* is partially responsible for CDK4/6 induced senescence. Importantly, we unveiled a correlation between the levels of *F9* and cancer progression studying different cancer-related datasets. Altogether, we believe *F9* could be considered as a potential biomarker to predict CDK4/6 inhibitor response when used as first-line treatment in cancer.

EXPERIMENTAL PROCEDURES

Cell culture

All cancer cell lines used in this study were obtained from American Type Culture Collection (ATCC) and were not authenticated upon arrival. Mycoplasma testing was performed. Human foreskin fibroblasts (HFFF2) were obtained from Culture Collections (Public Health England, UK). All cell lines were grown in high glucose Dulbecco's Modified Eagle Medium (DMEM) (Gibco) except for HCT-116, SK-OV-3, Capan2 and HT29 that were grown in McCoys 5a medium, SNU-387, NCI-H23, OVCAR-3 that were grown in RPMI and A549, PC-3 that were grown in F12K medium. All media was supplemented with 10% foetal bovine serum (FBS) (Thermo Fisher) and 1% of antibiotic-anti-mycotic (Thermo Fisher). Human umbilical vein endothelial cells (HUVEC) from pooled donors were purchased from Promocell (Heidelberg, Germany). The cells were grown in M199 (Life Technologies, Grand Island, NY) with 20% foetal bovine serum (Labtech, Heathfield, UK), 10U/ml heparin (Sigma, St. Louis, MO), and 30 μ g/ml endothelial cell

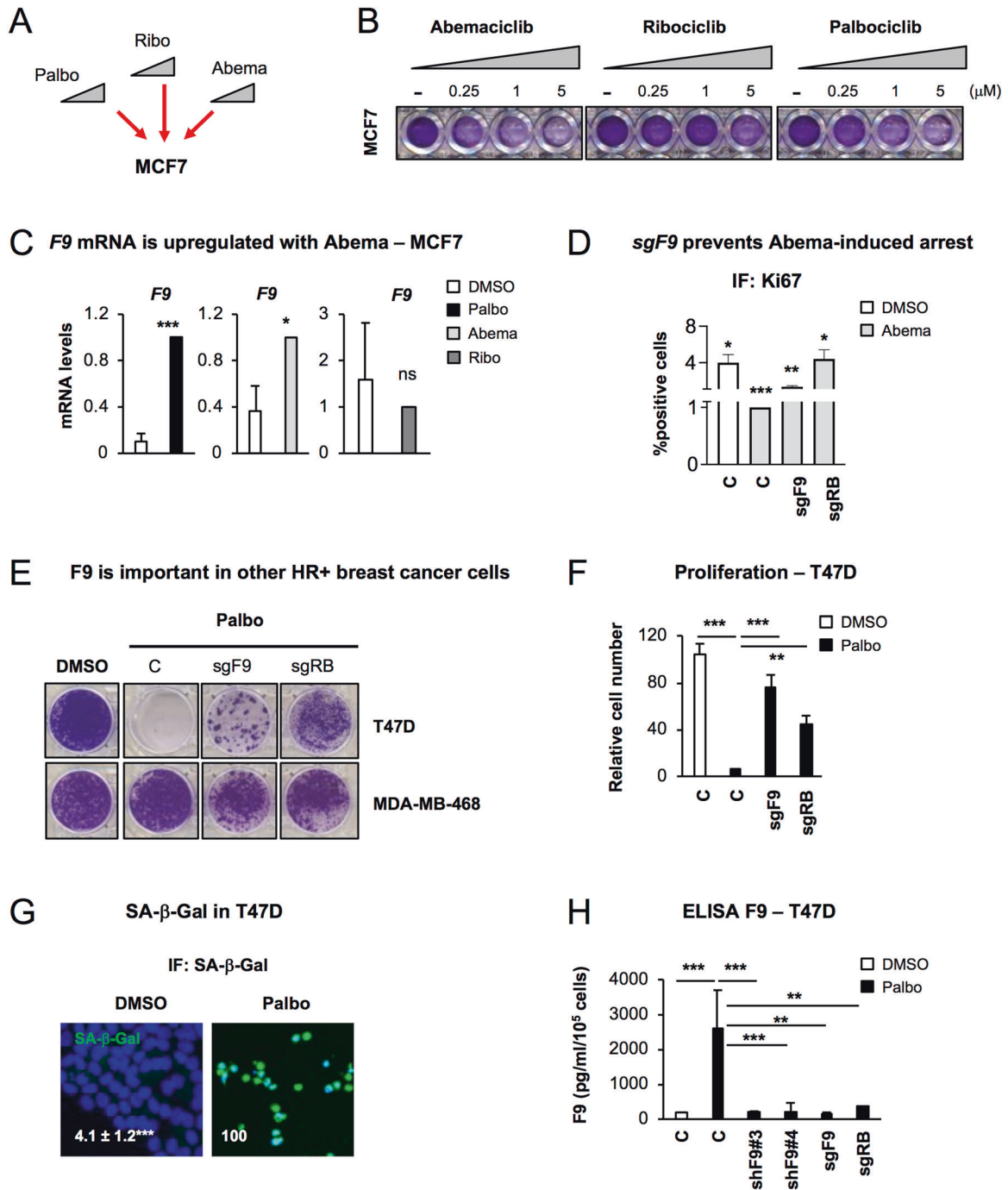


Fig. 4 CDK4/6 inhibitors induce a cell cycle arrest in different tumour types and is dependent on F9 in T47D cells. **A** Schematic representation of the treatment of MCF7 cells with 3 different CDK4/6 inhibitors: Palbociclib (Palbo), Ribociclib (Ribo) and Abemaciclib (Abema). **B** Colony formation assay stained with crystal violet for MCF7 treated with increasing concentrations of different CDK4/6 inhibitors for 10 days. A representative experiment is shown. **C** qPCR data show an upregulation of endogenous *F9* mRNA levels upon treatment with 500 nM Palbo, 500 nM Abema or 500 nM Ribo. Data show the mean \pm SEM of 3 independent experiments. Two-tailed *t*-test analysis is shown for statistical significance. **D** Ki67 proliferation assay in MCF7 cells expressing sgF9 or sgRB treated with 1 μ M Abema for 20 days. Representative experiment of 3 independent experiments is shown. Quantifications shows mean \pm SEM. Wilcoxon test analysis performed. **E** Crystal violet staining shows the effect on proliferation in T47D (ER⁺ breast cancer cells) and MDA-MB-468 (triple negative breast cancer cell line) expressing sgF9 or sgRB and treated with Palbo. Representative staining of 4 independent experiments is shown. **F** Relative cell count for T47D cells expressing either sgF9 or sgRB. Data show the mean \pm SEM of 7 independent experiments. One Way ANOVA with Dunnett's multiple comparisons to Palbo C sample was performed. **G** Representative pictures and quantification for number of cells presenting SA- β -Gal activity in T47D treated with 1 μ M Palbo for 20 days. Two-tailed student's *t*-test was performed. Scale bar: 50 μ m. **H** ELISA for human F9 released to the conditioned media in T47D cell treated with 1 μ M Palbo for 20 days expressing or not F9. sgRB is used as positive control. Data show mean \pm SEM of 3 independent experiments Two-tailed student's *t*-test was performed. Related to Fig. S4.

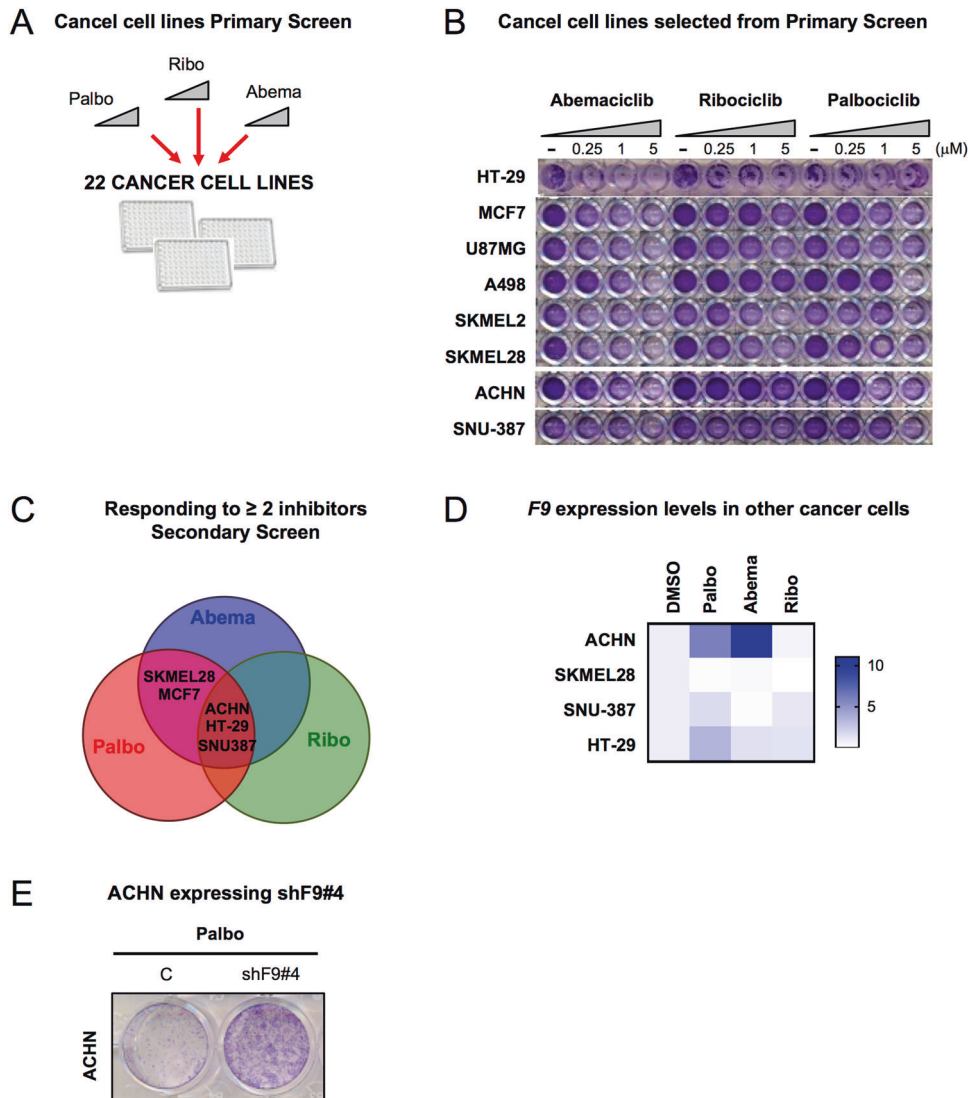


Fig. 5 CDK4/6 inhibitor response in a panel of different cancer cell lines. **A** A panel of 22 cancer cell lines of different origins were treated with increasing concentrations of Palbo, Ribo and Abema. **B** Crystal violet staining showing the 8 cancer cell lines that responded in a statistically significant ($p < 0.05$) and dose-dependent manner to more than 2 inhibitors. Representative experiment is shown. **C** Venn diagram shows that SKMEL28 (melanoma), MCF7 (breast cancer), ACHN (renal adenocarcinoma), HT-29 (colon) and SNU-387 (liver) cancer cell lines responded to two or more CDK4/6/ inhibitors ($p < 0.05$) in a Secondary Screen and were selected for further validation. **D** Heat map showing F9 mRNA expression in the indicated cancer cells after treatment with different CDK4/6 inhibitors. The map represents the mean of 3–5 independent replicates. **E** ACHN control or expressing shF9#4 stained with crystal violet after 20 days treatment with Palbo show a partial proliferation bypass. See also Fig. S5.

growth supplement (Sigma). Experiments were performed using HUVECs between passage 3 and 5.

Senescence induction

MCF7 cells were treated with different concentrations (100 nM, 200 nM, 500 nM or 1000 nM) of Palbociclib (PD0332991) (APEX-BIO), Abemaciclib (LY2835219) (Selleckchem) or Ribociclib (LEE011) (Selleckchem) and the other cancer cell lines with the indicated concentration of inhibitor. Media was changed every 2 days. Human primary fibroblasts (HFFF2) were treated with 50 μ M of Etoposide (Sigma-Aldrich) for 2 days and cells collected at day 7 or treated with 1 μ M Palbociclib for 7 days. HFFF2 expressing pLNC-ER:RAS vector, were induced to senescence by adding 200 nM 4-hydroxytamoxifen (4OHT) (Sigma-Aldrich) for 6 days. All treatments were done using DMEM supplemented with 10% FBS and 1% of antibiotic-anti-mycotic. HUVEC cells were treated with 500 nM Palbo for 7 days to induce senescence.

F9 recombinant experiments

Recombinant experiments were carried out by using F9 recombinant protein (R&D systems). MCF7 or SKMEL28 cancer cell lines were treated with 10 μ g/ml rF9 in complete medium for 72 hours with 2 treatments in total (6 days treatment). At the end of the experiment, cells were fixed with 4% paraformaldehyde (PFA) and used for immunofluorescence studies or stained for SA- β -Gal activity.

Retroviral and lentiviral infections

The generation of stable retroviral and lentiviral expression was carried out following previous studies [6, 12, 23, 45]. Briefly, retroviral particles were generated by transfecting pLNC-ER:H-RAS^{G12V} plasmid and retroviral helper plasmids (vsVg and gag-pol) with Polyethylenimine (PEI) in HEK293T packaging cells for 48 h. Recombinant lentiviral particles were generated using the second-generation packaging vectors psPAX2 and pMD2.G using PEI in HEK293T.

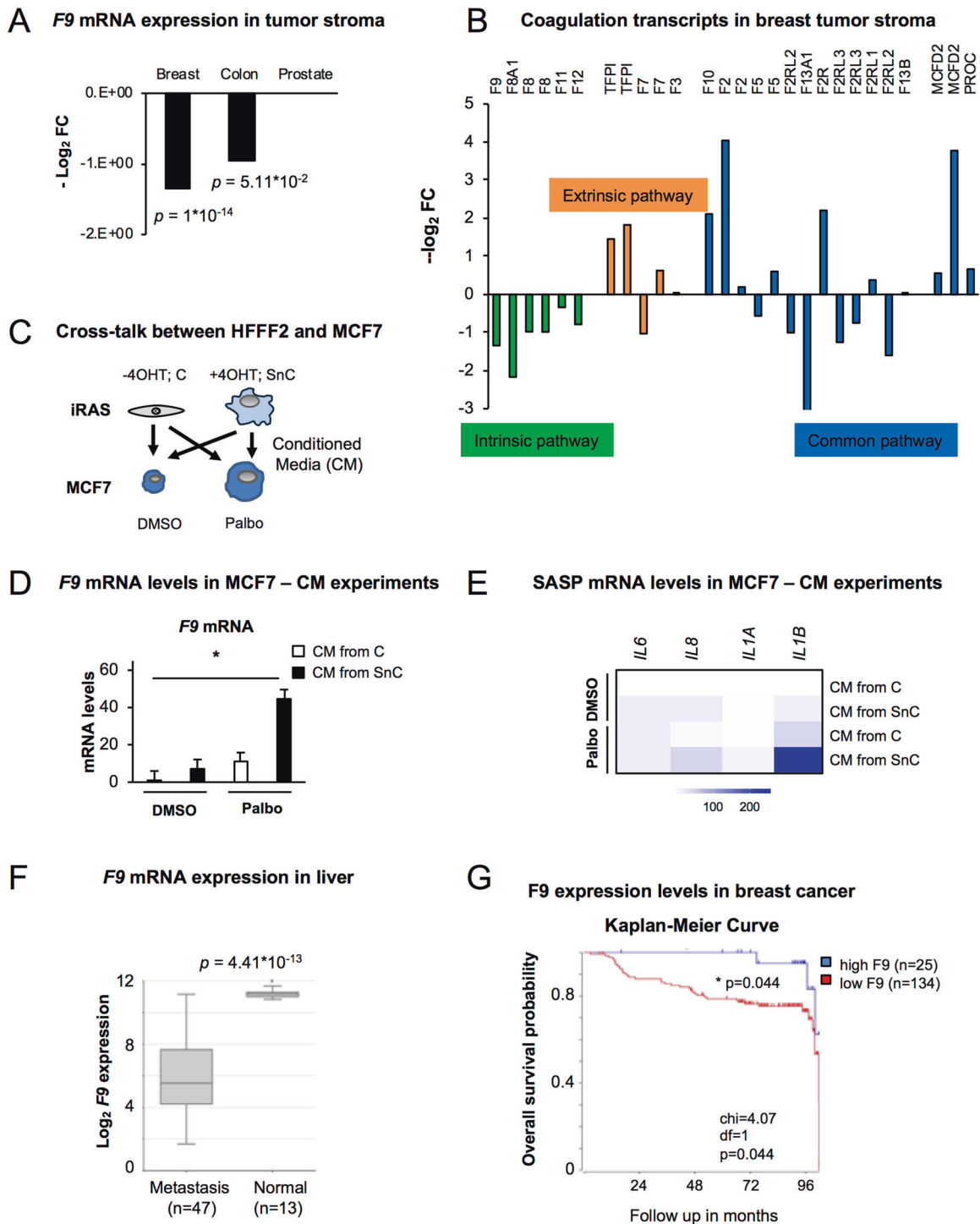


Fig. 6 *F9* expression is important in different tumours. **A** *F9* mRNA levels in tumour stroma vs healthy stroma in breast, colon and prostate cancers. Data are represented as $-\log_2$ fold change (FC) from [27]. Breast ($n = 12$ samples from normal versus $n = 111$ from tumour); colon ($n = 4$ samples from normal versus $n = 13$ from tumour); prostate ($n = 10$ samples from normal versus $n = 8$ from tumour). T-test student analyses is performed. **B** mRNA expression levels of different mRNA transcripts from genes implicated in the intrinsic coagulation pathway (green bars), extrinsic coagulation pathway (orange bars) and transcripts common to both pathways (blue bars) in breast cancer. Comparison of tumour stroma ($n = 111$) vs healthy stroma ($n = 12$) [27]. **C** Schematic representation of panels **D** and **E**. MCF7 cells pre-treated with DMSO or 500 nM Palbo were incubated for 72 h with the conditioned media (CM) of control (-4OHT) (C) or senescent (+4OHT) (SnC) iRAS HFFF2 primary fibroblasts. Senescence was induced with 200 nM 4OHT for 3 days, washed, incubated with fresh media and collected after 3 additional days. **D** *F9* mRNA levels and **E** heatmap for other SASP transcripts in MCF7 pre-treated with DMSO or 500 nM Palbo and incubated with the CM from iRAS (-/+ 200 nM 4OHT; C or SnC) for 72 h. Data show the mean \pm SEM of 4 independent replicates for *F9* and the mean of 4 independent experiments for the SASP. Two-way ANOVA with Dunnett's multiple comparisons analyses was performed. **F** *F9* mRNA expression levels in liver from normal ($n = 13$ samples) and metastatic ($n = 47$) liver. One-Way ANOVA analysis was performed to determine statistical significance. Dataset was calculated using R2. **G** Kaplan-Meier survival curve for high (blue) ($n = 25$) or low (red) ($n = 134$) *F9* expression levels and overall survival prognostic in breast cancer. Chi-square = 4.07; $p = 0.04$ [30]. Dataset calculated with R2.

The supernatant containing retrovirus or lentivirus was then filtered with 0.45 µm filters (Starlab) and applied to HFFF2 cells in the presence of 4 µg/ml polybrene (hexadimethrine bromide; Sigma-Aldrich) following 3 rounds of infection. Cells were subsequently selected with the appropriate antibiotic resistance either 0.5 µg/ml puromycin or 300 µg/ml neomycin (Invitrogen). For lentiviral infections with the sgRNA a pool for the 4 sgRNA (5 µg DNA per single sgRNA) targeting a single gene was generated by transfecting equal amounts of DNA and the packaging vectors psPAX2 and pMD2.G. Infection was performed as described earlier for lentivirus.

Genome-wide CRISPR/Cas9 library amplification and sequencing

The Human CRISPR knockout Pooled Library (GeCKOv2) was purchased from Addgene (#1000000048) and amplified using *E. coli* competent cells. The library contains 123,411 unique sgRNA sequences targeting 19,050 genes within the human genome. In order to maintain library representation and sufficient sgRNA coverage the library was amplified in large culture dishes (24 cm²) obtaining an approximate transformation efficiency of 4 × 10⁸ equivalent to ~10,000 colonies per sgRNA construct. After amplifying the library as described [20, 46], viral particles were produced in HEK293T cells and MCF7 cells were infected at a multiplicity of infection (MOI) of 0.2–0.5 following the lentiviral protocol previously described [20, 46]. Cells were selected with puromycin (1 µg/ml) for 72 h after the GeCKO library infection. After selection, cells were plated at low density and treated with 200 nM Palbociclib for 14 days to either determine proliferation or sent DNA for genomic DNA sequencing. Crystal violet staining was used to assess cell proliferation and determine the library bypass efficacy. After MCF7 cell infection and selection with the GeCKO library, genomic DNA was extracted at days 0 and day 14 after infection using the QIAmp Blood and Cell Culture DNA midi kit (Qiagen). The PCR was performed by QMUL Genome Centre. Analysis of genomic DNA at day 0 showed an sgRNA coverage higher than > 88%. The accession number for the sequencing data reported in this paper is GEO: GSE192525.

CRISPR sgRNA generation

The online guide design tool (<http://crispr.mit.edu>) was used to identify sgRNA sequences. The highest scoring guides were selected. Primers for the sgRNA sequences were ordered and the complementary sequences annealed at 37 °C for 30 min, followed by incubating the annealed primers at 95 °C for 5 min and then ramped down to 25 °C at 5 °C degrees per min. The annealed synthetic sgRNA oligonucleotides were cloned into pLenti-CRISPRv2 vector (Addgene #52961) at BsmBI restriction sites. The sgRNA sequences used in this study are:

```
sgF9#1GCAGCGCGTGAACATGATCATGG
sgF9#2CACTGAGTAGATATCCTAAAAGG
sgF9#3ATGATCATGGCAGAATCACCAGG
sgF9#4CTAAAAGGCAGATGGTGATGAGG
sgLPA5#1CCCAGAGGGCTAGCGCGTTGAGG
sgLPA5#2CCAGAGGGCTAGCGCGTTGAGGG
sgLPA5#3GGAAGATGGCGCCCTCGTCTGG
sgLPA5#4GCGTAGTAGGAGAGACGAACGGG
sgPROZ#1TGAGGGCTCCACACGATGGAGGG
sgPROZ#2GGTCTCGCCCTCCATCGTGTGG
sgPROZ#3CTGAGGGCTCCACACGATGGAGG
sgPROZ#4GCTCCACACGATGGAGGGGAGG
sgMOGAT#1CCGCAATGTAGTCCGAGAGGGG
sgMOGAT#2GCCCGCAATGTAGTCCGAGAGG
sgMOGAT#3GTTCCGAGTAACAGCGTGAAGG
sgMOGAT#4GCTGTTACTGCGGAACCGAAAGG
sgRB#3GGTGGCGGCCGTTTTTCGGGGGG
sgRB#4CGGCGGTGGCGCCGTTTTTCGG
```

To identify positive clones the primer hU6 CRISPR5'-GAGGGCCTATTTCCCATGATT-3' was used in combination with the reverse primer for each specific clone and isolated clones were SANGER sequenced.

Cell proliferation experiments

For cell proliferation studies, 100 cells were plated in each well of a 96-well plate and treated with CDK inhibitors (Palbociclib, Abemaciclib, Ribociclib) for 0, 6, 15, 20 days. The medium was replaced every other day either with drug or drug-free medium. For replating experiments, cells were treated with Palbociclib for 6 days, counted and replated at low density in a 96 well plate until day 20. Drug-withdrawal was performed by treating the cells 6 days in the presence of Palbociclib and removing the drug from day 6 to day 20. Cells were then fixed, stained with 0.5% crystal violet, solubilized with 30% acetic acid solution and absorbance was measured at 570 nm.

For colony formation assay, 5000 cells were plated in each well of a six-well plate, treated with CDK inhibitors 20–30 days (once control reached confluence). Cells were then washed with PBS, stained with crystal violet and scanned to obtain the pictures.

CDK4/6 inhibitors dose-response studies

Dose-response studies were carried out using the panel of cancer cell lines listed in the Cell Culture section. Cells were plated in a 96 well plate at 500–1000 cells/well (based on seeding density calculations) and treated with increasing concentrations (0.25–5 µM) of Palbociclib, Abemaciclib and Ribociclib. Medium containing the drugs or DMSO was replaced every other day during 10 days. The plates were then stained with 0.5% crystal violet solution and scanned. Crystal violet quantification was performed by solubilizing crystal violet staining with 30% acetic acid and measuring the absorbance at 570 nm.

β-galactosidase staining

Cells were washed with PBS and fixed with 0.05% (w/v) glutaraldehyde (in PBS) for 15 min at room temperature. Cells were washed a second time with PBS and incubated with 5-bromo-4-chloro-3-indolyl-beta-D-galacto-pyranoside (X-gal) solution for 1 h at 37 °C. Cells were imaged after 12–24 h using a light microscope (Nikon) at 20X magnification and single representative images of each well were taken. Fluorescent β-Galactosidase was performed according to the manufacturer's instructions using the following commercial kit (Sigma-Aldrich, #F2756). Briefly, 33 µM of the β-gal substrate C₁₂FDG (Fluorescein di-β-D-galactopyranose) (F2756 Sigma-Aldrich) was added to the cells for 8 h at 37 °C. After, the cells were washed with PBS and fixed with 4% PFA.

RNA extraction, cDNA synthesis and qPCR

Total RNA was extracted using TRIzol Reagent (ThermoFisher) according to the manufacturer's instructions. cDNA synthesis was performed using High Capacity cDNA Reverse Transcriptase kit (ThermoFisher). qPCR reactions were performed using SYBR Green PCR Master Mix (Applied Biosystems) on a 7500 Fast System RealTime PCR cycle (Applied Biosystems). Primer sequences used in this study are:

```
F9 Forward5'-CAGTGTTCAGAGCCAAGCAA-3'
F9 Reverse5'-CATGGTGAACACGAAACCAG-3'
PROZ Forward5'-CACCCCTGAGAAAGACTTCG-3'
PROZ Reverse5'-GGAGCCTCTGTGTTCTCTGG-3'
RB Forward5'-AACCAGGAAGGAATGGCT-3'
RB Reverse5'-CTGCGTTCAGGTATTGATG-3'
IL8 Forward5'-GAGTGGACCACTGCCGCA-3'
IL8 Reverse5'-TCCACAACCCTCTGCACCCAGT-3'
IL6 Forward5'-CCAGGAGCCCAGCTATGAAC-3'
IL6 Reverse5'-CCCAGGGAGAAGGCAACTG-3'
CCL20 Forward5'-GGGAATCAGAAGCAGCAAGCAAC-3'
CCL20 Reverse5'-ATTGGCCAGCTGCCGTGTGAA-3'
```

IL1A Forward5'-AGTGCTGCTGAAGGAGATGCCTGA-3'
 IL1A Reverse5'-CCCTGCCAAGCACACCCAGTA-3'
 IL1B Forward5'-TGCACGCTCCGGGACTCACA-3'
 IL1B Reverse5'-CATGGAGAACCACACTTGTGTCTCC-3'
 CDKN1A Forward5'-CCTGCTACTGTCTTGTACCCT-3'
 CDKN1A Reverse5'-GCGTTTGGAGTGGTAGAAATCT-3'
 ACTIN Forward5'-GCCCTGAGGCACTCTTCCA-3'
 ACTIN Reverse5'-CGGATGTCCACGTCACACTTC-3'
 RSP14 Forward5'-CTGCGAGTGTCTGTCAGAGG-3'
 RSP14 Reverse5'-TCACCGCCCTACACATAAACT-3'

Protein lysis and western blot

Cells were lysed in ice-cold Lysis Buffer 6 (R&D systems) supplemented with 10 μ L/mL of protease inhibitor cocktail. Total protein content was determined by Precision Red Reagent (Sigma) protein assay. Twenty micrograms of total protein were separated on 10% SDS-PAGE and transferred to a polyvinylidene fluoride (PVDF) membrane (Millipore Co., Bedford, MA). Protein transfer was checked by staining the membrane with Ponceau S red (Sigma-Aldrich). The membrane was then blocked using 5% bovine serum albumin (BSA) (Sigma) or 5% milk (Sigma) in PBS supplemented with 0.05% Tween-20 (Sigma) (PBST). Primary antibodies RB1 (BD; Cat# 554136) and β -Actin (Abcam, Cat# ab8226) were incubated overnight at 4 C. After four washes with PBST, the membrane was incubated with a secondary antibody for 1 h at room temperature. Protein bands were detected using SuperSignal West Pico PLUS Chemiluminescent Substrate (Thermo Fisher Scientific) using the ChemiDoc XRS + System (Bio-Rad).

Immunofluorescence

Cells were grown in a 96-well plate and fixed with 4% paraformaldehyde for 10 min at RT. Cells were then washed twice with PBS and permeabilized by incubating with 0.4% Triton X-100 in PBS for 10 min at RT. After a PBS wash, cells were blocked 30 min at RT using 1% BSA in PBS supplemented with 0.1% Tween-20 (PBST). Primary antibodies (details found at the end of the section) were diluted in 1% BSA-PBST and incubated overnight. For BrdU staining, cells were treated with DNaseI and MgCl₂ simultaneously with the primary antibody. Cells were then washed with PBS and incubated with their respective secondary antibody for 1 h at RT. Nuclei were stained with DAPI (Sigma-Aldrich). Images were acquired using INCell 2200 automated 991 microscope (GE) and INCell 2200 Developer software version 1.8 (GE) was used for image analysis. Antibodies used in this study are: p21^{CIP} (Abcam, Cat# ab109520), Ki67 (Abcam, Cat# ab92742), BrdU (Abcam, ab6326; 1:500) and F9 (Proteintech, Cat# 21481-1-AP).

Conditioned media experiments

Donor cells (HFF2 iRAS) were treated in the presence or absence of 200 nM 4-hydroxytamoxifen (4OHT) (Sigma-Aldrich) for 3 days, washed and replenished with fresh media to prevent carrying the 4OHT. Conditioned medium (CM) was collected and supplemented to 10% FBS and added to MCF7, T47D, SKMEL28 or MDA-MB-468 recipient cells for 72 h. MCF7 or MDA-MB-468 cells were pre-treated in the presence or absence of 500 nM Palbociclib prior to adding the CM.

When using MCF7 as donors, cells were treated in the presence or absence of 500 nM Palbociclib for 7 days. At day 7 Palbo was removed and DMEM 0.5% FBS was added for 72 h to collect the Conditioned medium (CM). CM was collected and supplemented to 10% FBS and added to recipient cells (MCF7, T47D, SKMEL28) for 72 h. Recipient cells were pre-treated prior to CM addition in the presence or absence of 500 nM Palbociclib.

ELISA

Quantitative analysis to determine the presence of Human Factor 9 was performed by evaluating the concentration of F9 in the conditioned media of different cell cultures using the Abcam

Human Factor IX ELISA Kit (ab108831). The amount of F9 was normalised to cell number at the end of each experiment.

Statistics

Dataset analysis were performed using R2: Genomics Analysis and Visualization Platform (<http://r2.amc.nl>). STRING interactions were identified using the functional protein association networks (<https://string-db.org/>). Kyoto Encyclopedia of Genes and Genomes (KEGG) pathway analysis was performed using Panther pathway analysis (<http://www.pantherdb.org>). All statistical analyses performed are specified in the figure legend. A $p < 0.05$ is considered significant throughout the paper as follows: * $p < 0.05$; ** $p < 0.01$; *** $p < 0.001$.

REFERENCES

- Wagner V, Gil J. Senescence as a therapeutically relevant response to CDK4/6 inhibitors. *Oncogene*. 2020;39:5165–76.
- Dorr JR, Yu Y, Milanovic M, Beuster G, Zasada C, Dabritz JH, et al. Synthetic lethal metabolic targeting of cellular senescence in cancer therapy. *Nature*. 2013;501:421–5.
- Spring LM, Wander SA, Andre F, Moy B, Turner NC, Bardia A. Cyclin-dependent kinase 4 and 6 inhibitors for hormone receptor-positive breast cancer: past, present, and future. *Lancet*. 2020;395:817–27.
- Salvador-Barbero B, Alvarez-Fernandez M, Zapatero-Solana E, El Bakkali A, Menendez MDC, Lopez-Casas PP, et al. CDK4/6 Inhibitors Impair Recovery from Cytotoxic Chemotherapy in Pancreatic Adenocarcinoma. *Cancer Cell*. 2020;38:584.
- Asghar U, Witkiewicz AK, Turner NC, Knudsen ES. The history and future of targeting cyclin-dependent kinases in cancer therapy. *Nat Rev Drug Disco*. 2015;14:130–46.
- Rapisarda V, Borghesan M, Miguela V, Encheva V, Sniijders AP, Lujambio A, et al. Integrin Beta 3 Regulates Cellular Senescence by Activating the TGF-beta Pathway. *Cell Rep*. 2017;18:2480–93.
- Ruscetti M, Morris JPT, Mezzadra R, Russell J, Leibold J, Romesser PB, et al. Senescence-Induced Vascular Remodeling Creates Therapeutic Vulnerabilities in Pancreas Cancer. *Cell*. 2020;181:424–41.e421.
- Lee S, Schmitt CA. The dynamic nature of senescence in cancer. *Nat Cell Biol*. 2019;21:94–101.
- Faget DV, Ren Q, Stewart SA. Unmasking senescence: context-dependent effects of SASP in cancer. *Nat Rev Cancer*. 2019;19:439–53.
- Coppe JP, Desprez PY, Krtolica A, Campisi J. The senescence-associated secretory phenotype: the dark side of tumor suppression. *Annu Rev Pathol*. 2010;5:99–118.
- Fafian-Labora JA, O'Loughlin A. Classical and Nonclassical Intercellular Communication in Senescence and Ageing. *Trends Cell Biol*. 2020;30:628–39.
- Borghesan M, Fafian-Labora J, Eleftheriadou O, Carpintero-Fernandez P, Paez-Ribes M, Vizcay-Barrera G, et al. Small Extracellular Vesicles Are Key Regulators of Non-cell Autonomous Intercellular Communication in Senescence via the Interferon Protein IFITM3. *Cell Rep*. 2019;27:3956–71.e3956.
- Demaria M, O'Leary MN, Chang J, Shao L, Liu S, Alimirah F, et al. Cellular Senescence Promotes Adverse Effects of Chemotherapy and Cancer Relapse. *Cancer Disco*. 2017;7:165–76.
- Hamm CA, Moran D, Rao K, Trusk PB, Pry K, Sausen M, et al. Genomic and Immunological Tumor Profiling Identifies Targetable Pathways and Extensive CD8 +/PDL1+ Immune Infiltration in Inflammatory Breast Cancer Tumors. *Mol Cancer Ther*. 2016;15:1746–56.
- Finn RS, Dering J, Conklin D, Kalous O, Cohen DJ, Desai AJ, et al. PD 0332991, a selective cyclin D kinase 4/6 inhibitor, preferentially inhibits proliferation of luminal estrogen receptor-positive human breast cancer cell lines in vitro. *Breast Cancer Res*. 2009;11:R77.
- Pandey K, An HJ, Kim SK, Lee SA, Kim S, Lim SM, et al. Molecular mechanisms of resistance to CDK4/6 inhibitors in breast cancer: A review. *Int J Cancer*. 2019;145:1179–88.
- Anders L, Ke N, Hydbring P, Choi YJ, Widlund HR, Chick JM, et al. A systematic screen for CDK4/6 substrates links FOXM1 phosphorylation to senescence suppression in cancer cells. *Cancer Cell*. 2011;20:620–34.
- Alvarez-Fernandez M, Malumbres M. Mechanisms of Sensitivity and Resistance to CDK4/6 Inhibition. *Cancer Cell*. 2020;37:514–29.
- Goel S, DeCristo MJ, McAllister SS, Zhao JJ. CDK4/6 Inhibition in Cancer: Beyond Cell Cycle Arrest. *Trends Cell Biol*. 2018;28:911–25.
- Shalem O, Sanjana NE, Hartenian E, Shi X, Scott DA, Mikkelsen T, et al. Genome-scale CRISPR-Cas9 knockout screening in human cells. *Science*. 2014;343:84–87.
- Wang T, Wei JJ, Sabatini DM, Lander ES. Genetic screens in human cells using the CRISPR-Cas9 system. *Science*. 2014;343:80–84.

22. Finn RS, Crown JP, Lang I, Boer K, Bondarenko IM, Kulyk SO, et al. The cyclin-dependent kinase 4/6 inhibitor palbociclib in combination with letrozole versus letrozole alone as first-line treatment of oestrogen receptor-positive, HER2-negative, advanced breast cancer (PALOMA-1/TRIO-18): a randomised phase 2 study. *Lancet Oncol.* 2015;16:25–35.
23. Fafian-Labora JA, Rodriguez-Navarro JA, O’Loghlen A. Small Extracellular Vesicles Have GST Activity and Ameliorate Senescence-Related Tissue Damage. *Cell Metab.* 2020;32:71–86.e75.
24. Ashida S, Orloff MS, Bebek G, Zhang L, Zheng P, Peehl DM, et al. Integrated analysis reveals critical genomic regions in prostate tumor microenvironment associated with clinicopathologic phenotypes. *Clin Cancer Res.* 2012;18:1578–87.
25. Finak G, Bertos N, Pepin F, Sadekova S, Souleimanova M, Zhao H, et al. Stromal gene expression predicts clinical outcome in breast cancer. *Nat Med.* 2008;14:518–27.
26. Nishida N, Nagahara M, Sato T, Mimori K, Sudo T, Tanaka F, et al. Microarray analysis of colorectal cancer stromal tissue reveals upregulation of two oncogenic miRNA clusters. *Clin Cancer Res.* 2012;18:3054–70.
27. Valencia T, Kim JY, Abu-Baker S, Moscat-Pardos J, Ahn CS, Reina-Campos M, et al. Metabolic reprogramming of stromal fibroblasts through p62-mTORC1 signaling promotes inflammation and tumorigenesis. *Cancer Cell.* 2014;26:121–35.
28. Acosta JC, O’Loghlen A, Banito A, Guijarro MV, Augert A, Raguz S, et al. Chemokine signaling via the CXCR2 receptor reinforces senescence. *Cell.* 2008;133:1006–18.
29. Sheffer M, Bacolod MD, Zuk O, Giardina SF, Pincas H, Barany F, et al. Association of survival and disease progression with chromosomal instability: a genomic exploration of colorectal cancer. *Proc Natl Acad Sci USA.* 2009;106:7131–6.
30. Pawitan Y, Bjohle J, Amler L, Borg AL, Eghyazi S, Hall P, et al. Gene expression profiling spares early breast cancer patients from adjuvant therapy: derived and validated in two population-based cohorts. *Breast Cancer Res.* 2005;7:R953–964.
31. Sanada F, Taniyama Y, Muratsu J, Otsu R, Shimizu H, Rakugi H, et al. Source of Chronic Inflammation in Aging. *Front Cardiovasc Med.* 2018;5:12.
32. Boccaccio C, Sabatino G, Medico E, Girolami F, Follenzi A, Reato G, et al. The MET oncogene drives a genetic programme linking cancer to haemostasis. *Nature.* 2005;434:396–400.
33. Ashrani AA, Gullerud RE, Petterson TM, Marks RS, Bailey KR, Heit JA. Risk factors for incident venous thromboembolism in active cancer patients: A population based case-control study. *Thromb Res.* 2016;139:29–37.
34. Zagar TM, Cardinale DM, Marks LB. Breast cancer therapy-associated cardiovascular disease. *Nat Rev Clin Oncol.* 2016;13:172–84.
35. Wiley CD, Liu S, Limbad C, Zawadzka AM, Beck J, Demaria M, et al. SILAC Analysis Reveals Increased Secretion of Hemostasis-Related Factors by Senescent Cells. *Cell Rep.* 2019;28:3329–37.e3325.
36. Acosta JC, Banito A, Wuestefeld T, Georgilias A, Janich P, Morton JP, et al. A complex secretory program orchestrated by the inflammasome controls paracrine senescence. *Nat Cell Biol.* 2013;15:978–90.
37. De Cecco M, Ito T, Petrashen AP, Elias AE, Skvir NJ, Criscione SW, et al. L1 drives IFN in senescent cells and promotes age-associated inflammation. *Nature.* 2019;566:73–78.
38. Wilkerson WR, Sane DC. Aging and thrombosis. *Semin Thromb Hemost.* 2002;28:555–68.
39. Franchini M. Hemostasis and aging. *Crit Rev Oncol Hematol.* 2006;60:144–51.
40. Sathyan S, Ayers E, Gao T, Milman S, Barzilai N, Verghese J. Plasma proteomic profile of frailty. *Aging Cell.* 2020;19:e13193.
41. Engbers MJ, van Hylckama Vlieg A, Rosendaal FR. Venous thrombosis in the elderly: incidence, risk factors and risk groups. *J Thromb Haemost.* 2010;8:2105–12.
42. Malehmir M, Pfister D, Gallage S, Szydłowska M, Inverso D, Kotsiliti E, et al. Platelet GPIIb/IIIa is a mediator and potential interventional target for NASH and subsequent liver cancer. *Nat Med.* 2019;25:641–55.
43. Heit JA, Mohr DN, Silverstein MD, Petterson TM, O’Fallon WM, Melton LJ 3rd. Predictors of recurrence after deep vein thrombosis and pulmonary embolism: a population-based cohort study. *Arch Intern Med.* 2000;160:761–8.
44. Mingozzi F, Liu YL, Dobrzynski E, Kaufhold A, Liu JH, Wang Y, et al. Induction of immune tolerance to coagulation factor IX antigen by in vivo hepatic gene transfer. *J Clin Invest.* 2003;111:1347–56.

45. Fafian-Labora J, Carpintero-Fernandez P, Jordan SJD, Shikh-Bahaei T, Abdullah SM, Mahenthiran M, et al. FASN activity is important for the initial stages of the induction of senescence. *Cell Death Dis.* 2019;10:318.
46. Sanjana NE, Shalem O, Zhang F. Improved vectors and genome-wide libraries for CRISPR screening. *Nat Methods.* 2014;11:783–4.

ACKNOWLEDGEMENTS

We want to thank the Queen Mary University of London Genome Centre, Dr. Luke Gammon and Dr. Gary Warnes for technical support. We thank Adrian Biddle for his help with the migration experiments. This paper was funded by the BBSRC (BB/P000223/1), the MRC (MR/K501372/1), The Royal Society (RG170399) and Barts Charity (MGU0497 and G-002158) grants to A.O. M.M. was funded by PI19/00145, IN607B2020/12 and 858014. J.F.L. is funded by Xunta de Galicia (ED481B 2017/117). M.B. was funded by MRC (MR/K501372/1). T.P.M. was funded by a QMUL PhD programme and T.D.N.’s lab is currently funded by a Barts Charity project grant (MGU0534). P.C.F. is currently funded by GAIN (IN606C 2021/006) Xunta de Galicia.

AUTHOR CONTRIBUTIONS

AO conceived and designed the entire study. PCF performed most of the experiments with the help of OE, BPC, JFL and AY. MB amplified the sgRNA library and carried out the GeCKOv2 whole genome wide screen. TPM and TDN performed the endothelial cells experiments. MDM and MO provided advice. PCF and AO designed the experiments and wrote the paper with input from all authors.

COMPETING INTERESTS

StarkAge Therapeutics helped with the revision of this paper by performing some of the experiments. B.P.C and M.O. are staff members at StarkAge Therapeutics. A.O. forms part of the StarkAge Therapeutics Scientific Advisory Board and has an unrelated project funded by StarkAge Therapeutics.

ADDITIONAL INFORMATION

Supplementary information The online version contains supplementary material available at <https://doi.org/10.1038/s41419-022-04569-3>.

Correspondence and requests for materials should be addressed to Ana O’Loghlen.

Reprints and permission information is available at <http://www.nature.com/reprints>

Publisher’s note Springer Nature remains neutral with regard to jurisdictional claims in published maps and institutional affiliations.



Open Access This article is licensed under a Creative Commons Attribution 4.0 International License, which permits use, sharing, adaptation, distribution and reproduction in any medium or format, as long as you give appropriate credit to the original author(s) and the source, provide a link to the Creative Commons license, and indicate if changes were made. The images or other third party material in this article are included in the article’s Creative Commons license, unless indicated otherwise in a credit line to the material. If material is not included in the article’s Creative Commons license and your intended use is not permitted by statutory regulation or exceeds the permitted use, you will need to obtain permission directly from the copyright holder. To view a copy of this license, visit <http://creativecommons.org/licenses/by/4.0/>.

© The Author(s) 2022